24

EIPS Beam Uniformity

John Everett

This chapter contains an overview of the Electron Impact Point Source (EIPS) Beam Uniformity (BU) measurements taken at XRCF and our analysis of them. (There were also DCM and HIREFS BU measurements taken, but those have been analyzed by the Project Science team, and their results are available from their web site at `http://wwwastro.msfc.nasa.gov/xray/xraycal/`. There appear to have been no BU tests taken with the Penning source.)

24.1   Beam Uniformity Tests

After each source and filter change at XRCF, a Beam Uniformity (BU) scan was taken to determine if the beam flux was non-uniform at the entrance aperture of the HRMA. The possibility of beam non-uniformity is important not only to tests that examine the response of different parts of the mirrors (such as shutter tests or Ring Focus measurements) but also to the use of the four Flow Proportional Counters (FPCs) in front of the HRMA for flux normalization: if there is a spatial non-uniformity in the beam, it is no longer strictly valid to find the flux at the face of the HRMA by averaging the flux detected in the four FPCs. One must employ a beam uniformity map to determine the actual flux 'seen' by the HRMA.

There were two different types of BU scans taken. The most accurate type of BU test was executed at the face of the HRMA with the "North" Flow Proportional Counter (one of the FPCs at the face of the HRMA; known as fpc_hn for Flow Proportional Counter at the HRMA, North). This detector carried out a 40 point scan with four points at the home positions of the fpc_h detectors, and the rest closely following the entrance apertures of the mirror shells. One can see this pattern in a plot from our analysis code, shown in Figure 24.1. fpc_hn had a 36 mm diameter hole defining its aperture for many of these BU scans. For some scans, the fpc_hn's fully open aperture was used, which caused problems when the open aperture extended beyond the X-ray beam at the fpc_ht and fpc_hb positions; those points have been identified and excluded from our analysis.

The second type of BU test was (commonly) a seven point scan done with the FPC in Building 500 (and therefore known as a FPC-500 scan), about 38 meters from the source building, and about 460 meters in front of the HRMA. These were fairly simple scans where two of the points coincided with the home positions of the fpc_5 and ssd_5 detectors with the other five sampling the main X-ray beam that would illuminate the HRMA. A sample FPC-500 beam scan is shown in
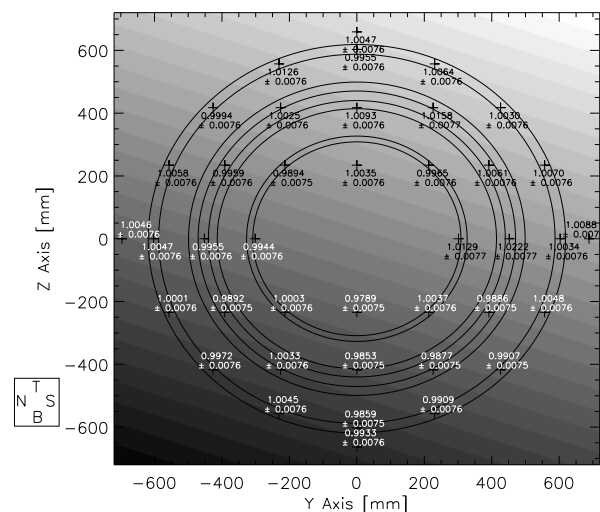
Figure 24.1: fpc_hn Scan Pattern with Polynomial Fit to Normalized Count Rates. The data was taken for MST Run ID 108363 (TRW ID D-BND-BU-2.038) on January 11, 1997 with the C-Kα EIPS anode. The concentric annuli represent the positions of the HRMA mirror shells.

Figure 24.2 (excluding the two data points taken out of the central X-ray beam). The fpc_5 used either the 4, 12, or 36 mm aperture for these scans.

24.2   Beam Uniformity Analysis

For our first cut at analyzing the BU data, we used the HXDS `.sum` files, which contain counts from each of the detectors (determined by a sum of all of the counts in a specified Region of Interest, or ROI) as well as live time information. After completing our 'quick-look' analysis using this method, we fit each of the spectra individually using XSPEC and JMKmod. For our XSPEC results, I heavily used the collection of XSPEC `.xcm` files that Dick Edgar has collected as a result of extensive XSPEC/JMKmod work.

An IDL program was developed that reads in the resultant count rates from either the HXDS `.sum` files or the XSPEC `.flux` files for the fpc_h and fpc_5 detectors, calculates the flux, and then determines a normalized flux. For the fpc_h tests, that normalized flux is derived by first taking the ratio of the fpc_h count rate to the fpc_5 count rate for each data point. The average of that normalized count rate is then calculated, and then divided back into the normalized count rate. Uncertainties are estimated using Poisson statistics.

For the FPC-500 scans, a second set of count rates is not available, so the program simply averages all of the fpc_5 count rates, and then divides the average into the all of count rates to derive a normalized count rate for each data point. This assumes that the source is constant in
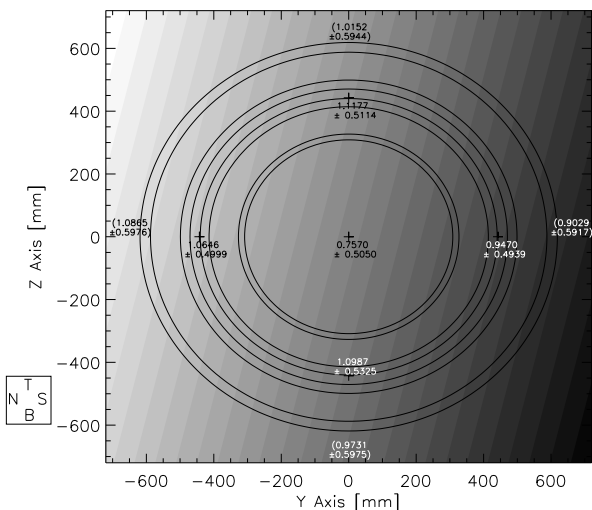
Figure 24.2: `fpc_5` Scan Pattern with Polynomial Fit to Normalized Count Rates. The data in this figure is from MST Run ID 110285 (TRW ID E-BND-BU-2.043) taken on January 28, 1997 with the C-Kα EIPS source. The program has extrapolated, from the polynomial fit, to predict values for the fluxes read at the home positions of the `fpc_h` detector home positions, indicated in parentheses.

time, but that seems to be true to high accuracy for almost all of the EIPS sources (except perhaps those with significant spectral contamination), and also, the FPC-500 scans were run for shorter integration (and overall) times than the FPC-HN scans, so time variability should be even less of a concern. As above, uncertainties are computed using Poisson statistics.

The program then projects the detector scan points back to the location of the HRMA entrance aperture and fits either a smoothed surface or a simple, first order polynomial over the data points, depending on user input. The smooth surface fit is found via an interpolation scheme that first tiles the coordinate grid with triangles whose vertices are data points, and then uses a fifth order polynomial fit to interpolate between the data points and extrapolate outside of the data (Akima, 1978). This produces a smooth surface that the program then uses to map out the flux as a function of mean mirror radius and azimuth. This method produces a map that very closely follows the data points, and was used initially as the basis for all of our BU analysis. These smooth fitting results are still available, although we almost exclusively use first order polynomials fits, now.

For fitting, the simplest function we can fit to the data is a single constant. We might hope that this constant would be the best fit, thus showing that the beam is indeed uniform within statistical uncertainty. We can compare that constant to fits of other functions that we might believe to be physically valid. For the Electron Impact Point Source (EIPS) and the Penning Source, the variations we might expect to see come mostly from some variation in the thickness of the filter in front of the source, which we might model with a simple slanted plane (in XRCF coordinates,

where y and z are in millimeters from the center of the HRMA, whose calculated position for each BU run is given in the buTableEIPS.rdb, an rdb table mentioned in more detail below):

$$(Normalized\ Count\ Rate)_i = a + by_i + cz_i$$

We have tried fitting this function to all of our analyzed EIPS data, and in many cases, it yields a χ_ν^2 close to unity. After this fit, the program then plots the fit as a function of mean mirror shell radius and azimuth, and also plots the data points that are close to that mirror shell, for comparison. Results for MST Run ID 112357 (TRW ID F-BND-BU-71.001, taken on February 25, 1997 with the Al-Kα EIPS anode) are shown below in Figures 24.3 through 24.5. The fits shown in those figures show a maximum variation of the fit of about 2.5 percent. This is actually very common for the EIPS BU maps: most fits vary only as much as 1 to 2 percent (two exceptions are MST Run IDs 110147 and 113089 (2.29 keV and 1.25 keV, respectively), which have much greater variations), and the maximum variation is usually found over the outermost shell, as one might expect.

Figure 24.3: Variation in fit and data points as a function of azimuth for mirror Shell 1. The data is from MST Run ID 112357 (TRW ID F-BND-BU-71.001), which was taken on February 25, 1997 with the Al-Kα EIPS anode.

The question still remains, however, of whether those equations actually fit the data any better (within statistical uncertainties) than a simple constant. We can apply the F test to determine whether the addition of the extra parameters in the above equations actually yields a better fit (Bevington and Robinson, 1992, pg. 208-209). For a catalog of all of our fits and F test results to present date, please see the BU webpage at URL

        `http://asc.harvard.edu/cal/Links/Compiled/hrma/bumap.html`.

All of our PostScript plots, as well as an rdb table (`buTableEIPS.rdb`) collecting all of the individual BU results, can be found on of this main web page. A listing of some of the columns from the rdb table is shown in Table 24.1.

Normalized Count Rate, Shells 3 and 4

Figure 24.4: Variation in fit and data points as a function of azimuth for mirror Shells 3 and 4. The data is from MST Run ID 112357 (TRW ID F-BND-BU-71.001), which was taken on February 25, 1997 with the Al-Kα EIPS anode.
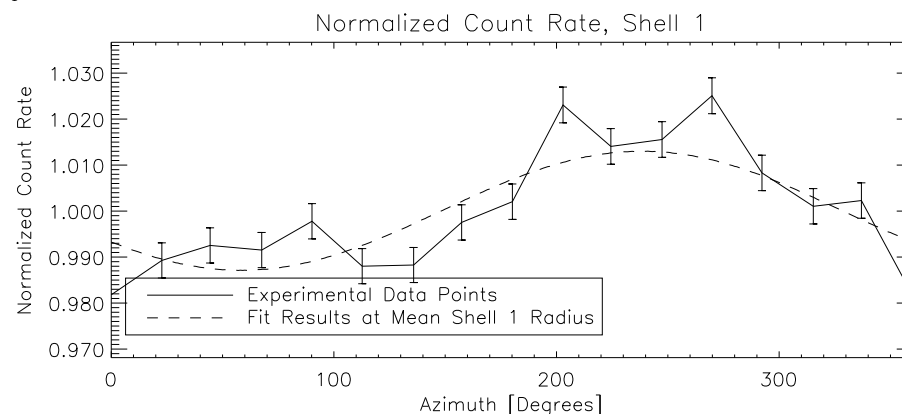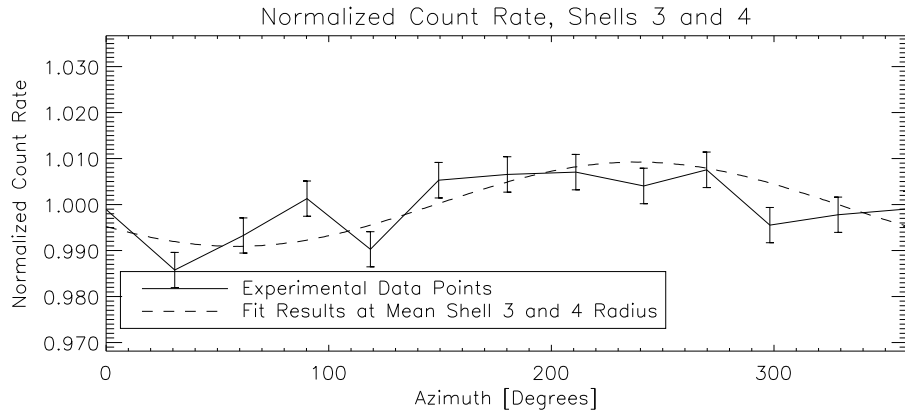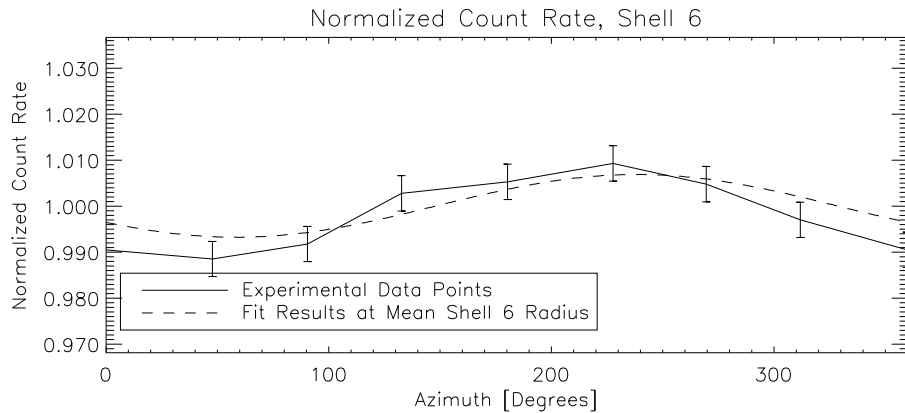
Normalized Count Rate, Shell 6

Figure 24.5: Variation in fit and data points as a function of azimuth for mirror Shell 6. The data is from MST Run ID 112357 (TRW ID F-BND-BU-71.001), which was taken on January 11, 1997 with the Al-Kα EIPS anode.

Table 24.1: Fit Results for all EIPS BU Tests. The results of the slanted-plane fits to all of the BU EIPS scans are presented in this table, along with F Test results for comparing constant fits to slanted plane fits. Of the two χ^2_ν values listed, the first ($\chi^2_{\nu,fit}$) is the χ^2_ν for the fit of the slanted plane, and the second ($\chi^2_{\nu,const}$) is the χ^2_ν for a constant value. For tests with F_χ greater than F_{upper}, the slanted plane gives a significantly improved fit over the simple constant.

TRW_ID	Energy	a	b	c	$\chi^2_{\nu,fit}$	$\chi^2_{\nu,const}$
		σ_a	σ_b	σ_c	F_χ	F_{upper}
C−BND−BU−2.035	1.490	1.00009	−3.40815e−05	2.64936e−06	2.905	4.298
		0.00282	1.01327e−05	1.00390e−05	3.919	99.000
C−BND−BU−2.036	1.490	1.00002	−1.14747e−05	−2.67304e−06	1.717	1.966
		0.00120	3.25334e−06	3.25856e−06	7.646	5.229
C−BND−BU−60.009	0.280	1.00046	7.49000e−05	8.89622e−06	0.792	2.277
		0.00769	2.74978e−05	2.75552e−05	9.496	99.000
C−BND−BU−60.010	0.280	1.00000	−1.18128e−06	2.79435e−06	0.974	0.927
		0.00330	8.93709e−06	8.95807e−06	0.118	5.229
C−BND−BU−60.007	1.490	1.00001	−7.75767e−06	9.68478e−06	1.833	1.284
		0.00287	1.02841e−05	1.02164e−05	0.801	99.000
C−BND−BU−60.008	1.490	1.00002	−9.50628e−06	−8.92112e−06	1.903	2.211
		0.00121	3.27804e−06	3.29079e−06	8.302	5.229
D−BND−BU−2.035	1.490	1.00002	−1.60653e−05	−4.77157e−06	0.468	1.007
		0.00267	9.53059e−06	9.55453e−06	6.600	99.000
D−BND−BU−2.036	1.490	1.00006	−1.87262e−05	−5.50266e−06	1.727	2.698
		0.00112	3.03715e−06	3.04106e−06	23.921	5.229
D−BND−BU−2.035a	1.490	1.00000	−7.25887e−06	−6.57621e−06	1.873	1.202
		0.00266	9.52932e−06	9.46761e−06	0.567	99.000
D−BND−BU−2.036a	1.490	1.00003	−8.53965e−06	−1.13365e−05	1.587	2.060
		0.00113	3.05151e−06	3.05394e−06	13.629	5.229
D−BND−BU−2.026	0.700	0.99998	2.50514e−06	1.18393e−05	1.448	1.386
		0.00540	1.42596e−05	1.57974e−05	0.408	5.268
D−BND−BU−2.028	6.400	1.00001	−6.54080e−06	5.91494e−06	1.755	1.738
		0.00193	5.27699e−06	5.21743e−06	1.614	5.229
D−BND−BU−2.025a	0.705	1.00003	1.19024e−05	−2.68191e−05	0.577	0.487
		0.00918	3.27523e−05	3.29316e−05	1.379	99.000
D−BND−BU−2.027	6.400	1.00000	9.08200e−06	−2.46893e−06	7.183	3.759
		0.00319	1.15067e−05	1.12980e−05	0.093	99.000
D−BND−BU−2.037	0.280	1.00000	−3.67794e−06	−2.62435e−07	0.533	0.295
		0.00308	1.10166e−05	1.09712e−05	0.210	99.000
D−BND−BU−2.038	0.280	1.00002	4.08737e−06	1.18176e−05	1.138	1.453
		0.00120	3.25662e−06	3.27716e−06	12.802	5.229
D−BND−BU−2.033	1.250	1.00002	−2.49726e−06	−1.75724e−05	0.940	0.815
		0.00422	1.50488e−05	1.51067e−05	1.469	99.000
D−BND−BU−2.034	1.250	1.00005	−9.73956e−06	−1.34318e−05	1.762	1.940
		0.00186	4.90488e−06	5.44204e−06	5.724	5.268
D−BND−BU−2.029	4.510	1.00000	1.10422e−05	1.10743e−05	1.811	2.346
		0.00182	6.53577e−06	6.49357e−06	3.182	99.000

Table 24.1: Fit Results for all EIPS BU Tests, continued.

TRW_ID	Energy	a	b	c	$\chi^2_{\nu,fit}$	$\chi^2_{\nu,const}$
		σ_a	σ_b	σ_c	F_χ	F_{upper}
D−BND−BU−2.030	4.510	0.99997	−1.64676e−06	4.26492e−06	0.776	0.808
		0.00101	2.72908e−06	2.73519e−06	3.598	5.229
D−BND−BU−2.007	0.520	1.00001	5.68058e−06	−2.87124e−06	0.470	0.705
		0.00130	4.63578e−06	4.65411e−06	4.007	99.000
D−BND−BU−2.001	0.930	1.00000	−1.00829e−05	8.18246e−06	1.760	1.174
		0.00336	1.19714e−05	1.20005e−05	0.667	99.000
D−BND−BU−2.003	8.030	1.00005	−1.19268e−05	2.99188e−05	0.370	1.346
		0.00418	1.49258e−05	1.49476e−05	12.544	99.000
D−BND−BU−2.004	8.030	1.00000	−8.48486e−07	7.40074e−06	1.029	1.023
		0.00189	4.98332e−06	5.49646e−06	1.791	5.268
D−BND−BU−2.020	3.440	0.99987	5.85193e−06	7.37793e−06	0.868	0.832
		0.00602	1.62181e−05	1.65826e−05	0.361	5.229
D−BND−BU−2.014	2.040	1.00373	2.28540e−05	4.10903e−05	21.851	22.984
		0.00184	4.62379e−06	5.37765e−06	3.712	5.362
D−BND−BU−2.013	2.040	1.00007	2.67702e−05	1.44823e−05	0.492	1.093
		0.00464	1.65118e−05	1.66111e−05	6.886	99.000
D−BND−BU−2.017	2.290	1.00002	−5.41036e−06	−2.00972e−05	1.342	1.157
		0.00417	1.47938e−05	1.49365e−05	1.449	99.000
D−BND−BU−2.018	2.290	1.00050	−4.53942e−05	−2.89089e−05	3.455	8.193
		0.00144	3.87923e−06	3.92420e−06	55.476	5.229
D−BND−BU−2.005	0.850	1.00001	4.94521e−06	−7.79643e−06	0.021	0.111
		0.00408	1.45812e−05	1.45812e−05	19.482	99.000
D−BND−BU−2.041	0.110	1.00016	−5.09332e−05	9.72039e−06	4.163	3.931
		0.00532	1.90605e−05	1.91309e−05	1.777	99.000
D−BND−BU−2.039	0.180	1.00003	−2.11774e−05	4.82300e−06	1.165	1.193
		0.00388	1.39015e−05	1.38396e−05	2.096	99.000
D−BND−BU−2.040	0.180	1.00000	1.64747e−06	1.60597e−06	1.255	1.199
		0.00129	3.41389e−06	3.75790e−06	0.331	5.268
E−BND−BU−2.043	0.277	1.00001	−1.88833e−06	−9.16368e−06	0.160	0.738
		0.00161	5.76348e−06	5.76616e−06	16.413	99.000
E−BND−BU−2.044	0.277	1.00001	−9.32083e−06	−2.12630e−06	1.609	1.691
		0.00140	3.77800e−06	3.78893e−06	3.980	5.229
E−BND−BU−2.027	6.400	1.00000	−5.71183e−06	−1.27929e−05	4.732	2.717
		0.00332	1.19438e−05	1.18052e−05	0.297	99.000
E−BND−BU−2.028	6.400	1.00000	−2.02997e−06	2.56462e−06	1.495	1.428
		0.00201	5.44052e−06	5.45186e−06	0.242	5.229
E−BND−BU−2.029	4.510	1.00006	1.35422e−05	2.67904e−05	0.026	1.364
		0.00362	1.29632e−05	1.29008e−05	206.730	99.000
E−BND−BU−2.030	4.510	1.00001	7.93309e−06	7.19870e−06	0.486	0.625
		0.00156	4.22701e−06	4.22119e−06	13.235	5.229
E−BND−BU−2.015	2.980	0.99998	4.18590e−06	−9.32613e−06	0.181	0.251
		0.00357	1.26866e−05	1.27888e−05	3.541	99.000
E−BND−BU−2.016	2.980	1.00000	−4.15124e−06	2.93009e−06	1.195	1.158

Table 24.1: Fit Results for all EIPS BU Tests, continued.

TRW_ID	Energy	a	b	c	$\chi^2_{\nu,fit}$	$\chi^2_{\nu,const}$
		σ_a	σ_b	σ_c	F_χ	F_{upper}
		0.00192	5.19438e−06	5.22246e−06	0.798	5.229
E−BND−BU−2.001	0.930	1.00000	−1.32484e−05	8.31557e−06	0.425	0.628
		0.00339	1.21639e−05	1.20843e−05	3.902	99.000
E−BND−BU−2.003	8.030	0.99994	9.74866e−06	−2.44388e−05	6.306	3.827
		0.00451	1.62158e−05	1.59987e−05	0.427	99.000
E−BND−BU−2.035	1.490	1.00005	−9.19765e−06	−2.15445e−05	0.674	3.435
		0.00186	6.66013e−06	6.65414e−06	18.372	99.000
E−BND−BU−2.023	5.410	1.00022	4.79380e−05	2.70673e−05	4.844	6.023
		0.00404	1.45592e−05	1.43369e−05	2.974	99.000
F−BND−BU−71.001	1.490	1.00007	−1.12402e−05	−1.82670e−05	2.608	6.928
		0.00061	1.62379e−06	1.62742e−06	66.600	5.229
F−BND−BU−71.002	0.930	1.00001	−1.98478e−06	6.29006e−06	1.351	1.680
		0.00069	2.56810e−06	2.55593e−06	4.924	7.559
F−BND−BU−71.003	8.030	1.00000	4.99967e−06	6.57708e−06	2.409	2.631
		0.00084	2.24960e−06	2.25276e−06	5.606	5.229
F−BND−BU−71.002a	0.930	1.00001	−5.42720e−06	3.81035e−06	0.522	0.964
		0.00071	2.63520e−06	2.63484e−06	12.133	7.559
F−BND−BU−71.003a	8.030	0.99999	1.15272e−06	2.98672e−06	1.280	1.239
		0.00123	3.25124e−06	3.28865e−06	0.744	5.229
F−BND−BU−71.008	6.400	1.00012	2.54596e−05	−2.25740e−05	4.173	6.310
		0.00134	3.55175e−06	3.57589e−06	21.974	5.229
F−BND−BU−71.009	0.700	1.00003	−1.59876e−05	−1.36148e−05	0.933	0.963
		0.00452	1.20756e−05	1.20788e−05	3.241	5.229
F−BND−BU−71.023	6.400	0.99376	5.99711e−05	−1.04384e−06	182.133	150.426
		0.00696	1.57501e−05	1.29900e−05	0.085	8.022
F−BND−BU−71.007	0.280	1.00000	−6.00555e−06	5.05003e−06	71.204	69.135
		0.00037	9.99948e−07	9.97364e−07	0.867	5.229
F−BND−BU−71.010	4.510	1.00004	1.17268e−07	9.81362e−06	0.673	0.708
		0.00230	6.83280e−06	5.95102e−06	4.041	5.229
F−BND−BU−71.011	0.450	1.00146	5.81334e−05	−1.56096e−04	0.698	1.138
		0.01714	6.35006e−05	6.42413e−05	9.569	7.559
F−BND−BU−71.006	0.520	1.00015	3.92564e−05	−8.36074e−06	1.545	1.611
		0.00635	1.69182e−05	1.69814e−05	3.648	5.229
F−BND−BU−71.005	1.740	1.00038	−3.49262e−05	4.89348e−05	2.118	3.865
		0.00265	7.06815e−06	7.06251e−06	34.148	5.229
F−BND−BU−71.013	0.850	1.00033	3.68032e−05	6.04605e−05	1.270	3.596
		0.00343	1.27796e−05	1.28204e−05	23.976	7.559
F−BND−BU−71.004	1.250	1.00158	3.73415e−05	−9.94471e−05	3.662	43.366
		0.00101	2.69061e−06	2.69081e−06	424.884	5.229
G−BND−BU−81.007	0.280	1.00003	−6.51892e−06	−1.47677e−05	1.180	1.463
		0.00165	4.39884e−06	4.41322e−06	11.370	5.229
G−BND−BU−81.022	0.110	1.00054	2.57768e−04	−3.46909e−04	0.179	2.518
		0.01827	9.62680e−05	1.81749e−04	41.218	4999.536

Table 24.1: Fit Results for all EIPS BU Tests, continued.

TRW_ID	Energy	a	b	c	$\chi^2_{\nu,fit}$	$\chi^2_{\nu,const}$
		σ_a	σ_b	σ_c	F_χ	F_{upper}
G−BND−BU−81.021	0.180	1.00001	−2.05933e−05	2.78142e−05	0.216	0.237
		0.01152	3.08143e−05	3.06438e−05	5.918	5.229
G−BND−BU−81.011	0.450	1.00057	−3.44642e−05	1.38253e−05	0.868	0.750
		0.01731	6.46812e−05	6.39322e−05	0.371	7.559
G−BND−BU−81.006	0.520	0.99992	−1.52032e−05	3.78581e−05	1.326	1.302
		0.01173	3.14650e−05	3.14308e−05	1.271	5.229
G−BND−BU−81.005	1.740	1.00028	−2.82025e−05	3.60225e−05	2.387	4.658
		0.00177	4.74495e−06	4.72368e−06	39.103	5.229
G−BND−BU−81.009	0.700	1.00271	2.45266e−04	6.46635e−05	2.223	2.453
		0.02606	6.96864e−05	6.93748e−05	6.040	5.229
G−BND−BU−81.013	0.850	1.00002	−5.01848e−06	5.97849e−06	0.673	0.682
		0.00251	6.43125e−06	6.48740e−06	2.155	7.559
G−BND−BU−81.002	0.930	1.00001	−9.88465e−06	−2.82025e−06	0.980	0.978
		0.00288	7.37642e−06	7.39165e−06	1.982	7.559
G−BND−BU−81.004	1.250	1.00005	−1.11282e−05	−2.02036e−05	1.062	1.911
		0.00145	3.88464e−06	3.88691e−06	33.189	5.229
I−BND−BU−2.022	1.740	1.00093	−1.77308e−05	3.12021e−05	9.370	30.440
		0.00108	2.63264e−06	2.29864e−06	24.486	8.649
I−BND−BU−2.008	0.520	1.00010	−9.36616e−07	−1.58046e−06	1.745	1.434
		0.00139	3.21912e−06	2.96713e−06	0.213	8.649
I−BND−BU−2.028	6.400	1.00008	−6.20802e−06	6.28369e−06	1.403	1.903
		0.00151	3.85321e−06	2.75128e−06	5.567	8.649
I−BND−BU−2.004	8.030	0.99996	−4.47744e−06	−3.83342e−07	5.261	4.451
		0.00109	2.90911e−06	2.20397e−06	0.460	8.649
I−BND−BU−2.030	4.510	0.99994	7.50034e−07	−8.42752e−07	0.550	0.448
		0.00180	4.77674e−06	3.65354e−06	0.143	8.649
I−BND−BU−2.016	1.490	1.00087	−2.15739e−05	−9.88483e−06	2.281	7.884
		0.00121	3.24823e−06	2.43388e−06	26.567	8.649
I−BND−BU−2.129	0.520	1.00723	−2.69526e−05	−1.21810e−04	1.208	1.103
		0.01019	2.35998e−05	2.49247e−04	1.130	8.649

24.3 Future Directions

Shortly, we will complete the first pass of analysis using XSPEC and JMKmod, and after that, the majority of BU analysis will be complete. Further analysis of the variation of the beam between tests, and the variation of a given EIPS flux over different BU tests, are possible future areas of concentration. Also, we may wish to try other fitting functions to improve the simple polynomial fits to the data. Comparisons of these BU maps with Phase I and J flat field calibration BU maps (which had higher statistics, although at fewer points) would be useful. In addition, we might improve the normalization statistics for our fpc_hn BU tests by including ssd_5 flux measurements when possible.

24.4 Acknowledgments